
You Only Sample Once: Taming One-Step Text-to-Image Synthesis by Self-Cooperative Diffusion GANs

Yihong Luo^{1,2}, Xiaolong Chen¹, Xinghua Qu³, Jing Tang^{1,2*}

¹ The Hong Kong University of Science and Technology (Guangzhou)

² The Hong Kong University of Science and Technology ³ Shanda Group

yluocg@connect.ust.hk, xchen738@connect.hkust-gz.edu.cn,
quxinghua17@gmail.com, jingtang@ust.hk

Abstract

We introduce **YOSO**, a novel generative model designed for rapid, scalable, and high-fidelity one-step image synthesis. YOSO integrates the diffusion process with GANs to achieve the best of two worlds. Specifically, we smooth the distribution by the denoising generator itself, performing self-cooperative learning. We show that our method can serve as a one-step generation model training from scratch with competitive performance. Moreover, we show that our method can be extended to finetune pre-trained text-to-image diffusion for high-quality one-step text-to-image synthesis even with LoRA fine-tuning. In particular, we provide the first diffusion transformer that can generate images in one step trained on 512 resolution, with the capability of adapting to 1024 resolution without extra explicit training.

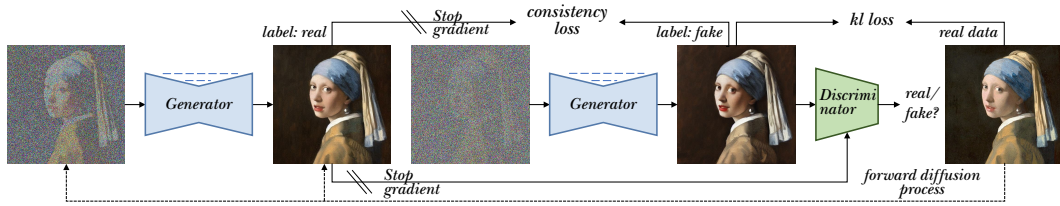
1 Introduction

Diffusion models (DMs) [12, 46, 50] have recently emerged as a powerful class of generative models, demonstrating state-of-the-art results in many generative modeling tasks, such as text-to-image [6, 7, 40, 60], text-to-video [4, 13], image editing [5, 9, 32] and controlled generation [33, 64]. However, the generation process of DMs requires iterative denoising, leading to slow generation speed. The sluggish generation time, coupled with the intensive computational requirements of large-scale DMs, constitutes a substantial barrier to their practical application and wider adoption.

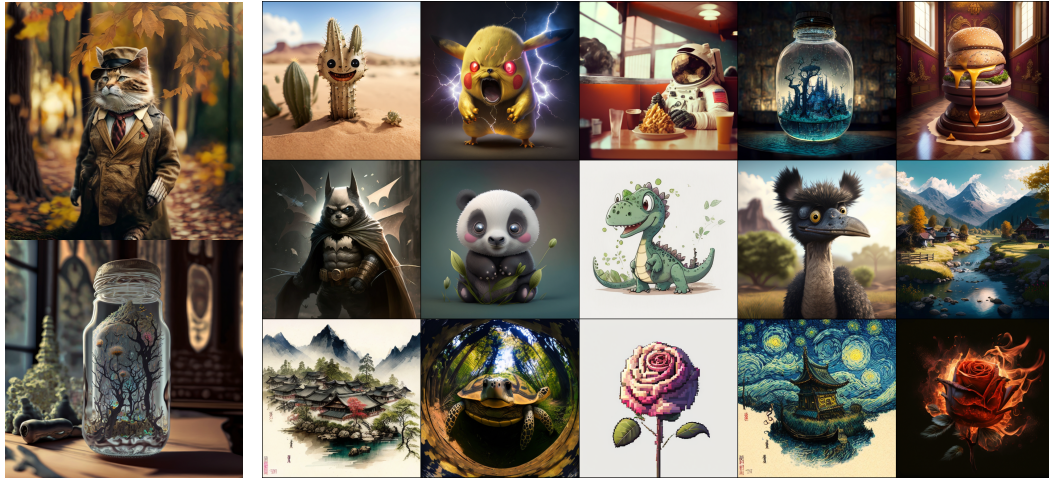
Sampling from DMs can be regarded as solving a probability flow ordinary differential equation (PF-ODE) [50]. Some previous works [2, 27, 28, 47] focus on developing advanced ODE-solver, for reducing the sampling steps. However, they still require 20+ steps to achieve high-quality generation. Another line is distilling from pre-trained PF-ODEs [26, 29, 30, 41, 49], aiming to predict multi-step solution of PF-ODE solver by one step. Existing methods [29, 30] can achieve reasonable sample quality with 4+ steps. However, it is still challenging to generate high-quality samples with one step.

In contrast, generative adversarial networks (GANs) [8, 38] are naturally built on one-step generation with fast sampling speed. However, it is hard to extend GANs on large-scale datasets due to the serious training challenges, with worse sample quality compared to DMs [17, 42]. In this work, we present a novel approach to combine diffusion process and GANs. Previous works [54, 59, 60] have developed some variants of diffusion-GAN hybrid models. However, they rely on adding noise to smooth the adversarial divergence, yielding indirect learning in the one-step generation. To directly learn the one-step generation by adversarial divergence and to avoid unstable learning, we propose defining the one-step generation distribution $p_\theta^{(t)}(\mathbf{x}) = \int q(\mathbf{x}_t)p_\theta(\mathbf{x}|\mathbf{x}_t)d\mathbf{x}_t$ on different levels of corrupted samples by diffusion process, where $q(\mathbf{x}_t)$ denotes the distribution of noisy data and $p_\theta(\mathbf{x}|\mathbf{x}_t)$ denotes the denoised distribution parameterized by denoising generator. Then, we

*Corresponding Author



(a) Framework of YOSO.



(b) 1024 resolution.

(c) 512 resolution.

Figure 1: **One-step** generated images by YOSO under different configurations (Bottom). The model is trained by fine-tuning PixArt- α [6] on 512 resolution with our proposed algorithm. Bottom Left is generated by YOSO adapting to 1024 resolution with Eq. (7) without extra explicit training.

regard the one-step generation based on less corrupted samples as ground truth to perform adversarial divergence. This approach can be regarded as a self-cooperative process, as the generator learns from itself. Such an innovative design enables stable training and effective learning for one-step generation. Hence, we name our model YOSO representing You Only Sample Once. Moreover, we extend our YOSO to one-step text-to-image generation based on pre-trained models by several effective training techniques (i.e., latent perceptual loss and latent discriminator for efficient training along with the latent DMs; the informative prior initialization (IPI), and the quick adaption stage for fixing the noise scheduler).

Thanks to our effective designs, we can efficiently and effectively fine-tune existing pre-trained text-to-image DMs (i.e., stable diffusion [40] and PixArt- α [6]) for high-quality one-step generation (See Fig. 1). Moreover, we are the first to support Low Rank Adaptation (LoRA) [16] fine-tuning for one-step generation of text-to-image.

Our work presents several significant contributions:

- We introduce YOSO, a novel generative model that can generate high-quality images with one-step inference.
- We propose several principled and effective training techniques enabling the fine-tuning of pre-trained text-to-image DMs for one-step text-to-image, requiring only ~ 10 A800 days.
- We develop the first one-step diffusion transformer [36] with PixArt- α , and the first LoRA enabling one-step generation, both of which will be released soon.
- We conduct extensive experiments to demonstrate the effectiveness of the proposed YOSO, including image generation from scratch, text-to-image generation fine-tuning, compatibility with existing image customization, and image controllable modules.

2 Related Works

Recently, several works have been developed for few-step text-to-image generation. LCM [29] adapts consistency distillation [49] for stable diffusion (SD) and enables image generation in 4

steps with acceptable quality. InstaFlow [26] adapts rectified flows [24, 25] for SD, facilitating the generation of text-to-image in a mere single step. Despite this, the fidelity of the generated images is still poor. DMD [62] adapts variation score distillation [52] for SD, which requires training an additional DMs for the generator distribution, akin to the discriminator in GANs. Recently, combining DMs and GANs for one-step text-to-image generation has been explored. UFOGen [60] extends DDGANs [54] and SSIDMs [59] to SD by modifying the computation of reconstruction loss from corrupted samples to clean samples. However, it still performs adversarial matching using corrupted samples. ADD [44] introduces a one-step text-to-image generation based on SD. It follows earlier research [43] by employing a pre-trained image encoder, DINOv2 [34], as the backbone of the discriminator to accelerate the training. However, the discriminator design moves the training from latent space to pixel space, which substantially heightens computational demands. Moreover, they directly perform adversarial matches at clean real data, increasing the challenge of training. This requires the need for a better but expensive discriminator design and expensive R1 regularization to stabilize the training. In contrast, we perform the adversarial training by replacing real data with self-generated data to smooth the ground truth. Moreover, compared with UFOGen and ADD, our approaches can be trained from scratch to perform one-step generation, which is not demonstrated by them. Additionally, we extend our method not only to SD but also to PixArt- α [6] which is based on diffusion transformer [36]. This demonstrates the wide application of our proposed YOSO.

3 Background

Diffusion Models. Diffusion models (DMs) [12, 46] define a forward process that gradually transforms samples from data distribution to Gaussian distribution by adding noise in T steps with variance schedule β_t : $q(\mathbf{x}_t|\mathbf{x}_{t-1}) \triangleq \mathcal{N}(\mathbf{x}_t; \sqrt{1-\beta_t}\mathbf{x}_{t-1}, \beta_t\mathbf{I})$. The corrupted samples can be directly obtained by $\mathbf{x}_t = \bar{\alpha}_t\mathbf{x}_0 + \sqrt{1-\bar{\alpha}_t}\epsilon$, where $\bar{\alpha}_t = \prod_{s=1}^t(1-\beta_s)$ and $\epsilon \sim \mathcal{N}(0, \mathbf{I})$. The parameterized reversed diffusion process is defined to gradually denoise: $p_\theta(\mathbf{x}_{t-1}|\mathbf{x}_t) \triangleq \mathcal{N}(\mathbf{x}_{t-1}; \mu_\theta(\mathbf{x}_t, t), \sigma_t^2\mathbf{I})$. The model can be trained by minimizing the negative ELBO [12, 20]: $\mathcal{L} = \mathbb{E}_{t, q(\mathbf{x}_0)q(\mathbf{x}_t|\mathbf{x}_0)} \text{KL}(q(\mathbf{x}_{t-1}|\mathbf{x}_t, \mathbf{x}_0) || p_\theta(\mathbf{x}_{t-1}|\mathbf{x}_t))$ where $q(\mathbf{x}_{t-1}|\mathbf{x}_t, \mathbf{x}_0)$ is Gaussian posterior derived in [12]. A key assumption in diffusion is that the denoising step size from t to $t-1$ is sufficiently small. This assumption ensures the true $q(\mathbf{x}_{t-1}|\mathbf{x}_t)$ follows Gaussian distribution, enabling the effectiveness of modeling $p_\theta(\mathbf{x}_{t-1}|\mathbf{x}_t)$ with Gaussian distribution.

Diffusion-GAN Hybrids. An issue in DMs is that the true $q(\mathbf{x}_{t-1}|\mathbf{x}_t)$ does not follow Gaussian distribution when the denoising step size is not sufficiently small. Therefore, in order to enable large denoising step size, Diffusion GANs [54] propose to minimize the adversarial divergence between model $p_\theta(\mathbf{x}'_{t-1}|\mathbf{x}_t)$ and $q(\mathbf{x}_{t-1}|\mathbf{x}_t)$: $\min_\theta \mathbb{E}_{q(\mathbf{x}_t)} [D_{\text{adv}}(q(\mathbf{x}_{t-1}|\mathbf{x}_t) || p_\theta(\mathbf{x}'_{t-1}|\mathbf{x}_t))]$, where $p_\theta(\mathbf{x}'_{t-1}|\mathbf{x}_t) \triangleq \int p_\theta(\mathbf{x}_0|\mathbf{x}_t)q(\mathbf{x}_{t-1}|\mathbf{x}_t, \mathbf{x}_0)d\mathbf{x}_0$ and $p_\theta(\mathbf{x}_0|\mathbf{x}_t)$ is imposed by a GAN generator. The capability of a GAN-based formulation, enables much larger denoising step sizes (i.e., 4 steps).

4 Method: Self-Cooperative Diffusion GANs

4.1 Revisiting of Diffusion GANs

A key issue in Diffusion-GAN hybrid models is that they match the generator distribution $p_\theta(\mathbf{x}_{t-1}|\mathbf{x}_t) \triangleq \mathbb{E}_{p_\theta(\mathbf{x}_0|\mathbf{x}_t)}q(\mathbf{x}_{t-1}|\mathbf{x}_t, \mathbf{x}_0)$ at corrupted data distribution. This formulation only indirectly learns the $p_\theta(\mathbf{x}_0|\mathbf{x}_t)$ and $p_\theta(\mathbf{x}_0) = \int q(\mathbf{x}_t)p_\theta(\mathbf{x}_0|\mathbf{x}_t)d\mathbf{x}_t$, which are the distributions used for one-step generation, making the learning process less effective.

4.2 Our Design

To enable more effective learning for one-step generation, we propose to directly construct the learning objectives over clean data. We first construct a sequence distribution of clean data as follows:

$$p_\theta^{(t)}(\mathbf{x}_0) = \int q(\mathbf{x}_t)p_\theta(\mathbf{x}_0|\mathbf{x}_t)d\mathbf{x}_t, \quad 0 < t \leq T; \quad p_\theta^{(0)}(\mathbf{x}_0) \triangleq q(\mathbf{x}_0), \quad (1)$$

where $q(\mathbf{x}_0)$ is the data distribution, $p_\theta(\mathbf{x}_0|\mathbf{x}_t) \triangleq \mathcal{N}(G_\theta(\mathbf{x}_t, t), \sigma^2\mathbf{I})$ and G_θ is the denoising generator. Note that $G_\theta(\mathbf{x}_t, t)$ is our denoising generator that predicts clean samples. If the network ϵ_θ is parameterized to predict noise, we have $G_\theta(\mathbf{x}_t, t) \triangleq \frac{\mathbf{x}_t - \sqrt{1-\bar{\alpha}_t}\epsilon_\theta(\mathbf{x}_t, t)}{\bar{\alpha}_t}$.

Given the constructed distribution, we can formulate the optimization objective as follows:

$$\begin{aligned} & \mathbb{E}_t[D_{\text{adv}}(q(\mathbf{x})||p_\theta^{(t)}(\mathbf{x})) + \lambda \cdot \text{KL}(q(\mathbf{x}_0, \mathbf{x}_t)||p_\theta(\mathbf{x}_0, \mathbf{x}_t))] \\ & = \mathbb{E}_t[D_{\text{adv}}(q(\mathbf{x})||p_\theta^{(t)}(\mathbf{x})) + \lambda_t \cdot \text{KL}(q(\mathbf{x}_0)q(\mathbf{x}_t|\mathbf{x}_0)||q(\mathbf{x}_t)p_\theta(\mathbf{x}_0|\mathbf{x}_t))], \end{aligned} \quad (2)$$

where $q(\mathbf{x}_0, \mathbf{x}_t) \triangleq q(\mathbf{x}_0)q(\mathbf{x}_t|\mathbf{x}_0)$ and $p_\theta(\mathbf{x}_0, \mathbf{x}_t) \triangleq q(\mathbf{x}_t)p_\theta(\mathbf{x}_0|\mathbf{x}_t)$. The optimization objective is constructed by the combination of adversarial divergence and KL divergence. Specifically, the adversarial divergence focuses on matching over the distribution level, ensuring the generation quality, and the KL divergence focuses on matching over point level, ensuring the mode cover.

However, it is hard to directly learn the adversarial divergence over clean data distribution, akin to the challenges with GAN training. To tackle these challenges, previous Diffusion GANs [54, 59] have pivoted towards learning the adversarial divergence over the corrupted data distribution. Unfortunately, as analyzed before, such an approach fails to directly match $p_\theta(\mathbf{x}_0)$, curtailing the efficacy of one-step generation. Moreover, it also compels the discriminator to fit different levels of noise, leading to limited capability.

Recall that $p_\theta^{(t)}(\mathbf{x})$ is defined as $\int q(\mathbf{x}_t)p_\theta(\mathbf{x}|\mathbf{x}_t)d\mathbf{x}_t$. The quality of the distribution has two key factors: 1) the ability of the trainable generator G_θ ; 2) the information given by \mathbf{x}_t .

Hence given the generator G_θ fixed, if we increase the information in \mathbf{x}_t , it is supposed that we can get a better distribution. In other words, it is highly likely that $p_\theta^{(t-1)}(\mathbf{x})$ is superior to $p_\theta^{(t)}(\mathbf{x})$. Motivated by the cooperative approach [11, 55–57] which uses an MCMC revised version of model distribution to learn the generator, we suggest to use $p_\theta^{(t-1)}(\mathbf{x})$ as ground truth to learn $p_\theta^{(t)}(\mathbf{x})$, which constructs the following training objective:

$$\min_\theta \mathcal{L}_\theta \triangleq \mathbb{E}_t \mathbb{E}_{q(\mathbf{x})q(\mathbf{x}_t|\mathbf{x})} \lambda_t \times \|G_\theta(\mathbf{x}_t, t) - \mathbf{x}\|_2^2 + \mathbb{E}_t(D_{\text{adv}}(p_\theta^{(t-1)}(\text{sg}(\mathbf{x}))||p_\theta^{(t)}(\mathbf{x}))), \quad (3)$$

where $\text{sg}[\cdot]$ denotes stop-gradient operator. This training objective can be regarded as a self-cooperative approach, since the ‘revised’ samples from $p_\theta^{(t-1)}(\mathbf{x})$ and samples from $p_\theta^{(t)}(\mathbf{x})$ are generated by the same network G_θ . Note that we only replace data distribution as $p_\theta^{(t-1)}(\mathbf{x})$ in the adversarial divergence for smoothing the learning objective, as recent work [31] has found that it is beneficial to learn the generator with a mix of real data and revised data.

In the distribution matching objective above, we apply the non-saturating GAN objective to minimize the adversarial divergence of marginal distributions. And the KL divergence for point matching can be optimized by L_2 loss. Hence a tractable training objective is formulated as follows:

$$\min_\theta \max_\phi \mathbb{E}_t [\mathbb{E}_{p_\theta^{(t-1)}(\mathbf{x})} \log D_\phi(\text{sg}(\mathbf{x}), t) - \mathbb{E}_{p_\theta^{(t)}(\mathbf{x})} \log D_\phi(\mathbf{x}, t)] + \lambda_t \mathbb{E}_{q(\mathbf{x})q(\mathbf{x}_t|\mathbf{x})} \|G_\theta(\mathbf{x}_t, t) - \mathbf{x}\|_2^2,$$

where D_ϕ is the discriminator network. We find that the self-cooperative approach is connected with Consistency Training [49]. However, Consistency Training considers the \mathbf{x}_{t-1} as an approximated ODE solution of \mathbf{x}_t to perform a point-to-point match. In contrast, our proposed objective matches $p_\theta^{(t)}(\mathbf{x})$ and $p_\theta^{(t-1)}(\mathbf{x})$ in marginal distribution level, which avoids the approximated error of ODE.

To further ensure the mode cover of the proposed model, we can add consistency loss to our objective as regularization, which constructs our final training objective:

$$\begin{aligned} & \min_\theta \max_\phi \mathbb{E}_t \left\{ \mathbb{E}_{p_\theta^{(t-1)}(\mathbf{x})} [\log D_\phi(\mathbf{x}, t) - \mathbb{E}_{p_\theta^{(t)}(\mathbf{x})} \log D_\phi(\mathbf{x}, t)] \right. \\ & \left. + \mathbb{E}_{q(\mathbf{x})q(\mathbf{x}_{t-1}|\mathbf{x})q(\mathbf{x}_t|\mathbf{x}_{t-1}, \mathbf{x})} [\lambda(t) \|G_\theta(\mathbf{x}_t, t) - \mathbf{x}\|_2^2 + \lambda_t^{\text{con}} \|G_\theta(\mathbf{x}_t, t) - \text{sg}(G_\theta(\mathbf{x}_{t-1}, t-1))\|_2^2] \right\}, \end{aligned} \quad (4)$$

5 Towards One-Step Text-to-Image Synthesis

Since training a text-to-image model from scratch is quite expensive, we suggest using pre-trained text-to-image DMs as initialization with Self-Cooperative Diffusion GANs. In this section, we introduce several principled designs for developing a generation model that enables one-step text-to-image synthesis based on pre-trained DMs.

5.1 Using pre-trained models for Training

Latent Perceptual Loss. Prior research [14, 15, 49] has confirmed the effectiveness of perceptual loss in various domains. Notably, recent studies [26, 49] has found that the LPIPS loss [65] is crucial

for obtaining few-step DMs with high sample quality. However, a notable drawback is that the LPIPS loss is computed in the data space, which is expensive. In contrast, the popular SD operate in the latent space to reduce computational demands. Hence, using LPIPS loss in training latent DMs is pretty expensive, as it requires not only the computation of LPIPS loss in the data space but also an additional decoding operation. Realizing that the pre-trained SD can serve as an effective feature extractor [58], we suggest using pre-trained SD to perform latent perceptual loss. However, SD is a UNet, whose final layer predicts epsilon with dimensions identical to the data. Hence we propose using the bottleneck layer of the UNet for computing:

$$d(\mathbf{z}_\theta, \mathbf{z}) = \|\text{HalfUNet}(\mathbf{z}_\theta, c, t = 0) - \text{HalfUNet}(\mathbf{z}, c, t = 0)\|_2^2, \quad (5)$$

where \mathbf{z} is the latent encoded images by VAE and c is the text feature. We note that the benefit of computing latent perceptual loss by SD is not only the computational efficiency but also the incorporation of text features, which are crucial in text-to-image tasks.

Latent Discriminator. Training GANs for the text-to-image on large-scale datasets faces serious challenges. Specifically, unlike unconditional generation, the discriminator for the text-to-image task should justify based on both image quality and text alignment. This challenge is more obvious during the initial stage of training. To address this issue, previous pure GANs [18] for text-to-image propose complex learning objectives and require expensive costs for training. The learning of GANs has been shown to benefit from using a pre-trained network as the discriminator. As discussed above, the pre-trained SD has learned representative features. Hence, we suggest applying the pre-trained SD for constructing the latent discriminator. Similar to latent perceptual loss, we only use half UNet for the discriminator followed by a simple predict head. The advantages of the proposed strategy are twofold: 1) we use the informative pre-trained network as initialization; 2) the discriminator is defined over latent space, which is computationally efficient. Unlike previous work [44] that defines a discriminator over data space which required decode latent and backward from decoder, yielding expensive computational cost. By applying the Latent Discriminator, we observe a stable training process with fast convergence. Note that, expensive R1 regularization is not needed in our approach.

Decoupled Scheduler. We find that the optimal scheduler for performing consistency loss and adversarial loss are not identical. Hence, to better unleash the capability of pre-trained DMs, we propose using decoupled schedulers to construct the following loss in fine-tuning pre-trained DMs:

$$\begin{aligned} \min_{\theta} \max_{\phi} \mathbb{E}_t \{ & \mathbb{E}_{p_{\theta}^{(t_k)}(\mathbf{z})} [\log D_{\phi}(\mathbf{z}, c, t) - \mathbb{E}_{p_{\theta}^{(t)}(\mathbf{z})} \log D_{\phi}(\mathbf{z}, c, t)] \\ & + \mathbb{E}_{q(\mathbf{z})q(\mathbf{z}_{t_m}|\mathbf{z})q(\mathbf{z}_t|\mathbf{z}_{t_m}, \mathbf{z})} [\lambda_t \|G_{\theta}(\mathbf{z}_t, c, t) - \mathbf{z}\|_2^2 + \lambda_t^{\text{con}} \|G_{\theta}(\mathbf{z}_t, c, t) - \text{sg}(G_{\theta}(\mathbf{z}_{t_m}, c, t_m))\|_2^2] \}, \end{aligned} \quad (6)$$

where $t_k = \max(t - k, 0)$, $t_m = \max(t - m, 0)$, and we let $k = 250$ and $m = 25$ in experiments.

5.2 Fixing the Noise Scheduler

A common issue in DMs is that the final corrupted samples are not pure noise. For example, the noise scheduler used by the SD makes the corrupted samples at the final timestep as: $\mathbf{x}_T = 0.068265 \cdot \mathbf{x}_0 + 0.99767 \cdot \epsilon$, where the terminal Signal-to-noise ratio (SNR) is $\frac{\bar{\alpha}_T}{1 - \bar{\alpha}_T} = 0.004682$, effectively creates a gap between training and inference. Previous work [23] has only observed that this makes DMs unable to produce pure black or white images. However, we find that this issue yields serious problems in one-step generation. As shown in Fig. 2, there are notable artifacts in one-step generation if we directly sample noise from standard Gaussian distribution. The reason may be that in multi-step generation, the gap can be gradually fixed in sampling, while one-step generation reflects the gap more directly. To address this issue, we provide two simple yet effective solutions.

Informative Prior Initialization (IPI). The non-zero terminal SNR issue is similar to prior hole issues in VAEs [3, 21, 22]. Therefore, we can use informative prior instead of non-informative prior to effectively address this issue. For simplicity, we adopt a learnable Gaussian Distribution $\mathcal{N}(\boldsymbol{\mu}, \sigma^2 \mathbf{I})$, whose optimal formulation is given below: $\epsilon'' = \bar{\alpha}_T \cdot (\mathbb{E}_{\mathbf{x}} \mathbf{x} + \text{Std}(\mathbf{x}) \times \epsilon') + \sqrt{1 - \bar{\alpha}_T} \cdot \epsilon$, where $\mathbb{E}_{\mathbf{x}} \mathbf{x}$ and $\text{Std}(\mathbf{x})$ can be efficiently estimated by finite samples, and ϵ' follows standard Gaussian distribution. As shown in Fig. 2, the artifacts in one-step generation are immediately removed after applying IPI. We note that the performance is achieved with minimal adjustment, enabling the possibility of developing one-step text-to-image generation by LoRA fine-tuning.



(a) w/o IPI (b) w/ IPI
Figure 2: Samples by YOSO-LoRA with one-step inference from different initialization.

Table 1: Unconditional generation results on CIFAR-10.

Model	FID↓	NFE↓	Time (s) ↓
YOSO	3.82	1	0.05
<i>Ablation:</i>			
YOSO w/o consistency loss	4.41	1	0.05
YOSO w/o LPIPS loss	4.63	1	0.05
YOSO w/ $D_{adv}(p_d p_\theta^t)$	10.85	1	0.05
UFOGen [60]	45.15	1	0.05
DDGANs [54]	3.75	4	0.21
CT [49]	8.70	1	-
iCT [48]	2.83	1	-
DDPM [12]	3.21	1000	80.5
EDM [19]	2.04	36	-
DDIM [47]	4.67	50	4.01
StyleGAN2 w/o ADA	8.32	1	0.04
StyleGAN2 w/ADA	2.92	1	0.04

Table 2: Training costs on CIFAR-10. * our re-production.

Model	Params (M)	BS×Iteration	FID↓
YOSO	61 ($G_\theta + D_\phi$)	256×200k	3.82
CT [49]	74	512×800k	8.70
CT* [49]	74	256×200k	16.51
iCT [48]	-	1024×400k	2.83
iCT* [48]	74	256×200k	15.28

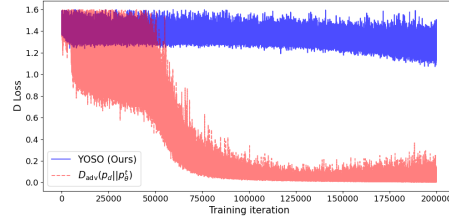


Figure 4: The discriminator loss curve.

Quick Adaption to v-prediction and Zero Terminal SNR. The IPI suffers from numerical instability when terminal SNR is pretty low. As shown in Fig. 3, we fine-tune PixArt- α [6] whose terminal SNR is $4e-5$ with introduced technique and ϵ -prediction, failing in one-step generation. Following [23], we suggest switching to v-prediction [41] and zero terminal SNR. However, we found that direct transition converges slowly (see Appendix F). This is unacceptable in solving large-scale text-to-image with limited computational resources. To address this, we propose a quick adapt-stage:

Figure 3: Predicting ϵ fails.

Adapt-stage-I switch to v-prediction : $L(\theta) = \lambda_t \|v_\theta(\mathbf{x}_t, t) - v_\phi(\mathbf{x}_t, t)\|_2^2$, where $v_\phi(\mathbf{x}_t, t) = \bar{\alpha}_t \epsilon_\phi(\mathbf{x}_t, t) - \sqrt{1 - \bar{\alpha}_t} \mathbf{x}_\phi^t$, $\mathbf{x}_\phi^t = \frac{\mathbf{x}_t - \sqrt{1 - \bar{\alpha}_t} \epsilon_\phi(\mathbf{x}_t, t)}{\bar{\alpha}_t}$, $v_\theta(\cdot, \cdot)$ denotes the desired v-prediction model, and $\epsilon_\phi(\cdot, \cdot)$ denotes the frozen pre-trained model.

Adapt-stage-II switch to zero terminal SNR : $L(\theta) = \lambda_t \|v_\theta(\mathbf{x}_t, t) - v_\phi(\mathbf{x}_t', t)\|_2^2$. Note that in this stage, we only change the scheduler to zero terminal SNR for student model. This avoids numerical instability issues of ϵ -prediction with zero terminal SNR. We note that the zero terminal SNR scheduler has lower SNR than the original schedule at each timestep, formulating an effective distillation objective.

We note that this adapt-stage converges rapidly, typically requiring only 1k iterations for training. This enables a quick adaption to v-prediction and zero terminal SNR from pre-trained ϵ -prediction DMs, thereby comprehensively mitigating the non-zero terminal SNR issue in the noise scheduler.

6 Experiments

In this section, we evaluate the performance of the proposed YOSO. In Sec. 6.1, we evaluate YOSO on unconditional image generation by training from scratch, and we conduct ablation studies in Sec. 6.2 to highlight the effectiveness of our algorithm. Sec. 6.3 examines YOSO in the context of text-to-image generation by fine-tuning pre-trained PixArt- α [6] and Stable Diffusion [40]. In Sec. 6.4, we show that the YOSO can be used for several downstream applications.

6.1 Unconditional Image Generation

Experiment Setting. We use the same UNet and discriminator architecture as used in DDGANs [54]. We set the denoising steps as four. For the evaluation metric, we choose the Fréchet inception distance (FID) [10]. We train the proposed model on the CIFAR-10 dataset [63]. Following Consistency Models [49], we employ LPIPS loss instead of MSE to compute image distance.

Results. The quantitative results are shown in Tab. 1. We observe that our method provides competitive performance compared with the best DMs and GANs. Although some variants of DMs achieve better results, they generally require much longer sample time compared to ours. We also find that among variants of GANs, our performance is surpassed only marginally by StyleGAN2 employing adaptive data augmentation. We also observe that the consistency models provide competitive and even better results compared to us. However, we note that the training of consistency models requires tons of computational resources and careful design of the noise schedule. As shown in

Table 3: Results of machine metrics with full fine-tuning on HPS benchmark.

Model	Params	Steps	HPS \uparrow	AeS \uparrow
SD 2.1-Turbo [44]	0.9B	1	27.06	5.83
SDXL-Turbo [44]	2.6B	1	<u>28.91</u>	5.84
InstaFlow [26]	0.9B	1	26.18	5.27
YOSO-PixArt- α	0.6B	1	29.83	<u>6.14</u>
YOSO-SD 1.5	0.9B	1	28.11	6.25

Table 4: Results of machine metrics with LoRA fine-tuning on HPS benchmark.

Model	Params	Steps	HPS \uparrow	AeS \uparrow
SD 1.5 [40]	0.9B	25	24.72	5.49
LCM-LoRA [30]	0.9B	2	19.77	5.25
LCM-LoRA [30]	0.9B	4	22.77	5.44
YOSO-LoRA	0.9B	1	23.34	<u>5.73</u>
YOSO-LoRA	0.9B	2	<u>23.91</u>	5.84

Tab. 2, the consistency models require much more computational resources than ours, including more parameters, larger batch size, and more training iterations. To ensure a fair comparison, we re-produce the consistency models by using the same batch size and training iterations as ours. Based on the fair setting, we find that the performance of consistency models significantly decrease, showing way worse performance compared to YOSO. We highlight that the low demand for computational resources enables us to scale the proposed YOSO to large-scale text-to-image datasets.

6.2 Ablation Studies

We provide additional insight into the effectiveness of the proposed YOSO by performing ablation studies to some potential variants on CIFAR-10 dataset.

Effect of Consistency Loss and LPIPS Loss. We evaluate the effect of consistency loss and LPIPS loss in YOSO. We find that both consistency loss and LPIPS loss can improve the image quality, as indicated by FID (see Tab. 1). However, we notice that if removing consistency loss or LPIPS loss, the generation performance would not decrease significantly. This indicates the effectiveness of our proposed adversarial formulation.

Adversarial Divergence $D_{\text{adv}}(p_d||p_\theta^t)$. The key design of our proposed YOSO is smoothing the distribution by using self-generated data instead of real data as ground truth to perform adversarial divergence. We evaluate the variant of using $D_{\text{adv}}(p_d||p_\theta^t)$ as adversarial divergence. As shown in Tab. 1, the performance of the variant is significantly worse than YOSO. Moreover, besides sample quality, we find that the training of our proposed YOSO is much more stable than the variant. As shown in Fig. 4, the discriminator loss of the variant is not stable and is much smaller than ours. This indicates that our approach can effectively smooth the distribution to make the distributions of fake and real samples closer to each other, making discrimination harder and hence resulting in higher discriminator loss. Furthermore, we observe mode collapse in the training of the variant. We note that a similar case also happened in SDXL-Turbo, a strong one-step text-to-image model, which also performs adversarial divergence directly against real data (See Fig. 5). These results indicate the superiority of the proposed YOSO.

Comparison to UFOGen. Similar to us, UFOGen does not directly perform adversarial divergence against real data either. However, they perform adversarial divergence over corrupted data (i.e., $D_{\text{adv}}(q(\mathbf{x}_{t-1})||\int q(\mathbf{x}_{t-1}|\mathbf{x} = G_\theta(\mathbf{x}_t, t))q(\mathbf{x}_t)d\mathbf{x}_t)$). We argue that the formulation is less effective in constructing one-step generation model since their adversarial divergence only indirectly matches the one-step generation at clean data. We implement the UFOGen on CIFAR-10 with our own. Note that we also perform consistency loss in the UFOGen variant to ensure a fair comparison, as the consistency loss has been found useful in YOSO. As shown in Tab. 1, UFOGen only obtains 45.15 FID on CIFAR-10, significantly worse than YOSO with 3.82 FID. This further demonstrates the superiority of our proposed YOSO. Through comparison with different adversarial divergence formulations, we find that our formulated adversarial divergence not only smooths the distribution to stabilize the training but also provides effective learning on one-step generation.

6.3 Text-to-Image Generation

Experiment Setting. We initialize the GAN generator by pre-trained PixArt- α which is a diffusion transformer with 0.6B parameters. We note that 0.6B parameters can be demonstrated as lightweight among text-to-image DMs. For the GAN discriminator, we construct the latent discriminator by pre-trained SD 1.5 using the proposed construction introduced in Sec. 5.1. We switch the pre-trained PixArt- α to v-prediction by the proposed technique introduced in Sec. 5.1, followed by training on the JourneyDB dataset [35] with resizing as 512 resolution. We apply a batch-size of 256 and a constant learning rate of $2e-5$ during training. We observe the training convergence fast, requiring only 30k iterations and around **10 A800 days** to be trained.

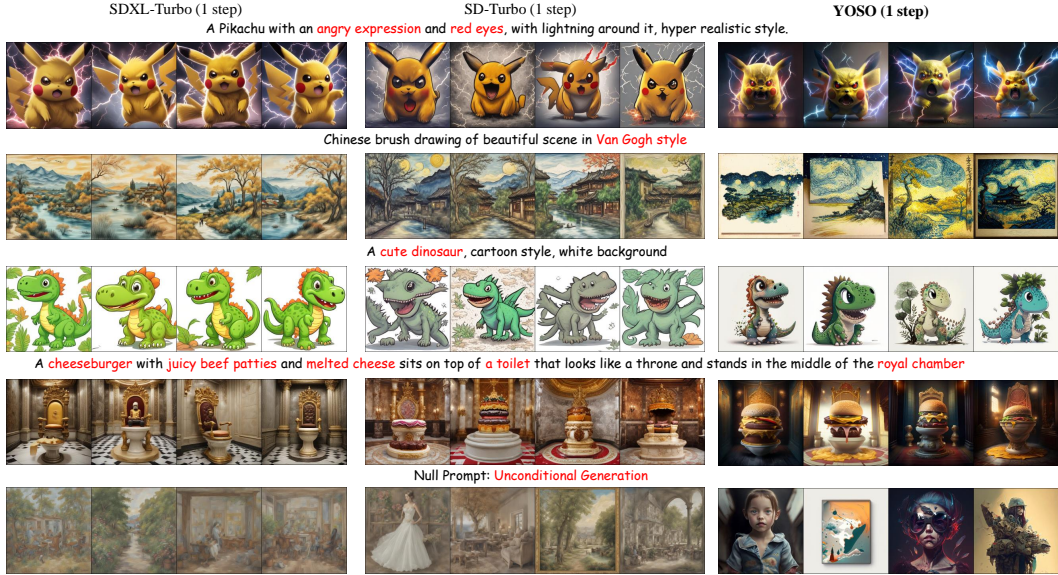


Figure 5: Qualitative comparisons of YOSO against competing methods. Zoom-in for better viewing.

Evaluation. For image quality, we employ Aesthetic Score (AeS) [45] to evaluate. We also adopt the Human Preference Score (HPS) v2.1 [53] to evaluate the image-text alignment and human preference. The AeS is computed by an aesthetic score predictor trained on LAION [45] datasets, without considering the image-text alignment. HPS is trained to predict human preference given image-text pairs, considering the image-text alignment and human aesthetic. We mainly compare our model against the open-source state-of-the-art (SOTA) models, i.e., SD-Turbo [44] and SDXL-Turbo [44].

Quantitative Results. The quantitative results are presented in Tab. 3. To provide a direct comparison with SD-Turbo, we also fine-tune a model based on pre-trained SD 1.5 on JourneyDB with the introduced technique. We would like to highlight that it is better to conduct training on LAION dataset [45] which is the training set used by SD 1.5. However, it is not available when we conducted this research. Fine-tuning SD 1.5 on other datasets suffers from distribution shift, facing a risk of catastrophic forgetting. As shown in Tab. 3, both YOSO-SD and YOSO-PixArt- α clearly beat the SD-Turbo which is based on SD 2.1, a better SD compared to SD 1.5. It is also observed that YOSO-PixArt- α outperforms SDXL-Turbo which is a much larger model with 2.6B parameters.

Qualitative Comparison. To provide more comprehensive insight in understanding the performance of our YOSO, we further provide the qualitative comparison in Fig. 5. The comparison shows that: YOSO clearly beats SD-Turbo in terms of both image quality and prompt alignment. Specifically, the samples by SD-Turbo are blurry to some extent. Although SDXL-Turbo with a larger model size improves the sample quality compared to SD-Turbo, we find that the samples by YOSO are sharper than SDXL-Turbo to some extent, and better in prompt alignment. For example, in the first row of Fig. 5 related to a Pikachu, both SD-Turbo and SDXL-Turbo cannot follow the prompt to generate angry expressions and red eyes, while YOSO follows the prompt more precisely. Moreover, it is important to highlight that SDXL-Turbo seems to have a serious issue in *mode collapse*. Specifically, the third row of Fig. 5 shows that samples by SDXL-Turbo are really close to each other. Overall, based on quantitative and qualitative results, we conclude that our YOSO is better in sample quality, prompt alignment, and mode cover compared with the SOTA one-step text-to-image models.

6.3.1 Zero-Shot One-Step 1024 Resolution Generation

Due to the computational resource limitation, we trained YOSO on 512 resolution. However, there is a 1024-resolution version of PixArt- α , obtained by continuing training on the 512-resolution version of PixArt- α . Motivated by the effectiveness of the LoRA combination [30], we suggest constructing a similar combination as follows:

$$\mathbf{W}_{\text{YOSO}_{1024}} = \mathbf{W}_{\text{PixArt}_{512}} + \alpha \cdot (\mathbf{W}_{\text{PixArt}_{1024}} - \mathbf{W}_{\text{PixArt}_{512}}) + \beta \cdot (\mathbf{W}_{\text{YOSO}_{512}} - \mathbf{W}_{\text{PixArt}_{512}}), \quad (7)$$

where $\alpha, \beta \in (0, 1]$ and \mathbf{W} means the model weight. We let $\alpha = \beta = 1$ in our experiments. As shown in Fig. 1b, the YOSO constructed in this way can generate high-quality images with 1024

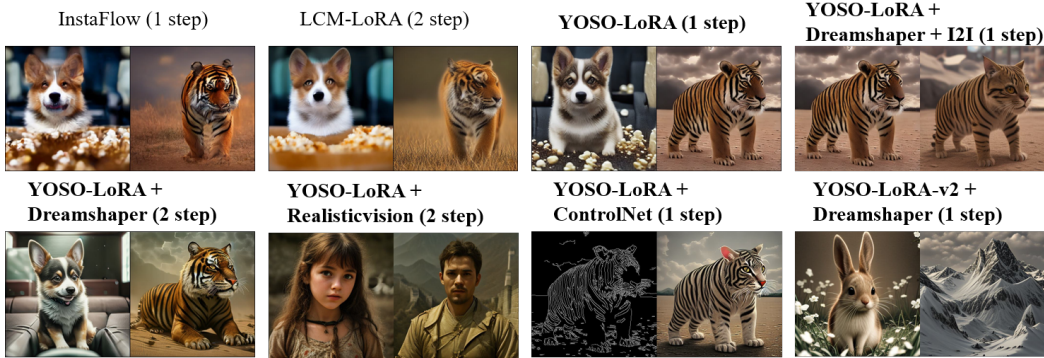


Figure 6: Qualitative comparison against competing methods and applications in down-stream tasks.

resolution. Note that YOSO even changes the predicted objective to v-prediction. The impressive performance indicates the robust generalization ability of our proposed YOSO.

6.3.2 Fine-tuning Stable Diffusion via LoRA

We further conduct experiments on fine-tuning SD 1.5 via LoRA to show the effectiveness of proposed YOSO. As we perform LoRA fine-tuning, it is expected that it will be worse than full fine-tuning, we propose to use SDXL-Turbo to generate data for LoRA fine-tuning, which avoids the risk of distribution shift to some extent and is economically efficient. We call the model fine-tuned in this way as YOSO-LoRA. We only generate one image for each caption, avoiding the risk of mode collapse brought by SDXL-Turbo. We train YOSO-LoRA with only 64 batch size and 4000 iterations. We present the quantitative results in Tab. 4 and qualitative results in Fig. 6. It can be observed that YOSO-LoRA achieves even better results than LCM with 4 steps and is comparable to InstaFlow with full fine-tuning. And from Fig. 6, YOSO-LoRA has a clearly better sample quality than LCM with 2 steps and InstaFlow. These results indicate that our algorithm enables one-step text-to-image synthesis with reasonable quality by LoRA fine-tuning.

6.4 Application

One promising and attractive property of DMs is that they can be used in multiple downstream tasks. In this section, we show the capability of our proposed YOSO in various downstream tasks, keeping the unique advantages of DMs. Since the relevant applications are mostly developed for SD, we mainly show the results obtained by YOSO-LoRA.

Image-to-image. As shown in Fig. 6, our YOSO-LoRA is capable of performing high-quality image-to-image editing [32] in one step.

Compatibility with ControlNet and Different Base Models. As shown in Fig. 6, our YOSO-LoRA is compatible with ControlNet [64], following the condition well. Our YOSO-LoRA is also compatible with different base models (e.g., dreamshaper and realistic vision) fine-tuned from SD 1.5, preserving their style well. We find that when applying YOSO-LoRA to new base models, it fails to produce reasonable samples in one step. This may be due to the capability of LoRA and the distribution shift of training data.

Enabling Data Flywheel. YOSO-LoRA trained on the data generated by SDXL-Turbo, fails to generate reasonable samples in one step when compatible with new base models. In light of the fact that combining YOSO-LoRA with new base models can generate high-quality samples in 4 steps with minimal performance loss as well as preserved style, we propose using YOSO-generated data for training YOSO-LoRA based on existing community models (e.g., Realistic-vision). We call the trained model YOSO-LoRA-v2. As shown in Tab. 5, YOSO-LoRA-v2 can even outperform the full fine-tuned SD-2.1-Turbo in one step. This shows that the YOSO can be trained on slightly shifted data first, and then applied to generate high-quality un-shifted data to train a better YOSO. Moreover, the YOSO-LoRA-v2 can be compatible with some unseen base models (e.g., Dreamshaper) for one-step generation (see Fig. 6 and Tab. 5). This shows

Table 5: Results of machine metrics.

Model	NFE	HPS \uparrow	AeS \uparrow
SD 2.1-Turbo [44]	1	27.06	5.83
Realistic-vision	50	29.76	6.35
w/ YOSO-LoRA	4	29.50	6.21
w/ YOSO-LoRA-v2	1	27.13	6.12
w/ YOSO-LoRA-v2	2	29.41	6.33
Dreamshaper			
w/ YOSO-LoRA-v2	1	26.64	6.08

that combining YOSO-LoRA with community models can generate unshifted training data, enabling the YOSO-LoRA-v2 to focus on learning the acceleration with better compatibility.

7 Conclusion

In summary, we present YOSO, a new generative model enabling high-quality one-step generation. Our novel designs combine the diffusion process and GANs, enabling not only one-step generation training from scratch but also one-step text-to-image generation fine-tuning from pre-trained models. We will release our model to advance the research of text-to-image synthesis.

References

- [1] Yogesh Balaji, Seungjun Nah, Xun Huang, Arash Vahdat, Jiaming Song, Karsten Kreis, Miika Aittala, Timo Aila, Samuli Laine, Bryan Catanzaro, et al. ediffi: Text-to-image diffusion models with an ensemble of expert denoisers. *arXiv preprint arXiv:2211.01324*, 2022.
- [2] Fan Bao, Chongxuan Li, Jun Zhu, and Bo Zhang. Analytic-dpm: an analytic estimate of the optimal reverse variance in diffusion probabilistic models. *arXiv preprint arXiv:2201.06503*, 2022.
- [3] Matthias Bauer and Andriy Mnih. Resampled priors for variational autoencoders. In Kamalika Chaudhuri and Masashi Sugiyama, editors, *The 22nd International Conference on Artificial Intelligence and Statistics, AISTATS 2019, 16-18 April 2019, Naha, Okinawa, Japan*, volume 89 of *Proceedings of Machine Learning Research*, pages 66–75. PMLR, 2019.
- [4] Andreas Blattmann, Tim Dockhorn, Sumith Kulal, Daniel Mendeleevitch, Maciej Kilian, Dominik Lorenz, Yam Levi, Zion English, Vikram Voleti, Adam Letts, Varun Jampani, and Robin Rombach. Stable video diffusion: Scaling latent video diffusion models to large datasets, 2023.
- [5] Tim Brooks, Aleksander Holynski, and Alexei A Efros. Instructpix2pix: Learning to follow image editing instructions. In *Proceedings of the IEEE/CVF Conference on Computer Vision and Pattern Recognition*, pages 18392–18402, 2023.
- [6] Junsong Chen, Jincheng YU, Chongjian GE, Lewei Yao, Enze Xie, Zhongdao Wang, James Kwok, Ping Luo, Huchuan Lu, and Zhenguo Li. Pixart- α : Fast training of diffusion transformer for photorealistic text-to-image synthesis. In *The Twelfth International Conference on Learning Representations*, 2024.
- [7] Zhida Feng, Zhenyu Zhang, Xintong Yu, Yewei Fang, Lanxin Li, Xuyi Chen, Yuxiang Lu, Jiaxiang Liu, Weichong Yin, Shikun Feng, Yu Sun, Li Chen, Hao Tian, Hua Wu, and Haifeng Wang. Ernie-vilg 2.0: Improving text-to-image diffusion model with knowledge-enhanced mixture-of-denoising-experts, 2023.
- [8] Ian Goodfellow, Jean Pouget-Abadie, Mehdi Mirza, Bing Xu, David Warde-Farley, Sherjil Ozair, Aaron Courville, and Yoshua Bengio. Generative adversarial nets. *Advances in neural information processing systems*, 27, 2014.
- [9] Amir Hertz, Ron Mokady, Jay Tenenbaum, Kfir Aberman, Yael Pritch, and Daniel Cohen-Or. Prompt-to-prompt image editing with cross attention control. *arXiv preprint arXiv:2208.01626*, 2022.
- [10] Martin Heusel, Hubert Ramsauer, Thomas Unterthiner, Bernhard Nessler, and Sepp Hochreiter. Gans trained by a two time-scale update rule converge to a local nash equilibrium. *Advances in neural information processing systems*, 30, 2017.
- [11] Mitch Hill, Erik Nijkamp, Jonathan Craig Mitchell, Bo Pang, and Song-Chun Zhu. Learning probabilistic models from generator latent spaces with hat EBM. In Alice H. Oh, Alekh Agarwal, Danielle Belgrave, and Kyunghyun Cho, editors, *Advances in Neural Information Processing Systems*, 2022.
- [12] Jonathan Ho, Ajay Jain, and Pieter Abbeel. Denoising diffusion probabilistic models. *Advances in neural information processing systems*, 33:6840–6851, 2020.

- [13] Wenyi Hong, Ming Ding, Wendi Zheng, Xinghan Liu, and Jie Tang. Cogvideo: Large-scale pretraining for text-to-video generation via transformers. *arXiv preprint arXiv:2205.15868*, 2022.
- [14] Yedid Hoshen, Ke Li, and Jitendra Malik. Non-adversarial image synthesis with generative latent nearest neighbors. In *Proceedings of the IEEE/CVF Conference on Computer Vision and Pattern Recognition*, pages 5811–5819, 2019.
- [15] Xianxu Hou, Linlin Shen, Ke Sun, and Guoping Qiu. Deep feature consistent variational autoencoder. In *2017 IEEE winter conference on applications of computer vision (WACV)*, pages 1133–1141. IEEE, 2017.
- [16] Edward J Hu, Yelong Shen, Phillip Wallis, Zeyuan Allen-Zhu, Yuanzhi Li, Shean Wang, Lu Wang, and Weizhu Chen. LoRA: Low-rank adaptation of large language models. In *International Conference on Learning Representations*, 2022.
- [17] Minguk Kang, Jun-Yan Zhu, Richard Zhang, Jaesik Park, Eli Shechtman, Sylvain Paris, and Taesung Park. Scaling up gans for text-to-image synthesis. In *Proceedings of the IEEE Conference on Computer Vision and Pattern Recognition (CVPR)*, 2023.
- [18] Minguk Kang, Jun-Yan Zhu, Richard Zhang, Jaesik Park, Eli Shechtman, Sylvain Paris, and Taesung Park. Scaling up gans for text-to-image synthesis, 2023.
- [19] Tero Karras, Miika Aittala, Timo Aila, and Samuli Laine. Elucidating the design space of diffusion-based generative models. In *Proc. NeurIPS*, 2022.
- [20] Diederik Kingma, Tim Salimans, Ben Poole, and Jonathan Ho. Variational diffusion models. *Advances in neural information processing systems*, 34:21696–21707, 2021.
- [21] Durk P Kingma, Tim Salimans, Rafal Jozefowicz, Xi Chen, Ilya Sutskever, and Max Welling. Improved variational inference with inverse autoregressive flow. *Advances in neural information processing systems*, 29:4743–4751, 2016.
- [22] Alexej Klushyn, Nutan Chen, Richard Kurlle, Botond Cseke, and Patrick van der Smagt. Learning hierarchical priors in vaes. In Hanna M. Wallach, Hugo Larochelle, Alina Beygelzimer, Florence d’Alché-Buc, Emily B. Fox, and Roman Garnett, editors, *Advances in Neural Information Processing Systems 32: Annual Conference on Neural Information Processing Systems 2019, NeurIPS 2019, December 8-14, 2019, Vancouver, BC, Canada*, pages 2866–2875, 2019.
- [23] Shanchuan Lin, Bingchen Liu, Jiashi Li, and Xiao Yang. Common diffusion noise schedules and sample steps are flawed. In *Proceedings of the IEEE/CVF Winter Conference on Applications of Computer Vision (WACV)*, pages 5404–5411, January 2024.
- [24] Qiang Liu. Rectified flow: A marginal preserving approach to optimal transport. *arXiv preprint arXiv:2209.14577*, 2022.
- [25] Xingchao Liu, Chengyue Gong, et al. Flow straight and fast: Learning to generate and transfer data with rectified flow. In *The Eleventh International Conference on Learning Representations*, 2022.
- [26] Xingchao Liu, Xiwen Zhang, Jianzhu Ma, Jian Peng, and Qiang Liu. InstafLOW: One step is enough for high-quality diffusion-based text-to-image generation. *arXiv preprint arXiv:2309.06380*, 2023.
- [27] Cheng Lu, Yuhao Zhou, Fan Bao, Jianfei Chen, Chongxuan Li, and Jun Zhu. Dpm-solver: A fast ode solver for diffusion probabilistic model sampling in around 10 steps. *Advances in Neural Information Processing Systems*, 35:5775–5787, 2022.
- [28] Cheng Lu, Yuhao Zhou, Fan Bao, Jianfei Chen, Chongxuan Li, and Jun Zhu. Dpm-solver++: Fast solver for guided sampling of diffusion probabilistic models. *arXiv preprint arXiv:2211.01095*, 2022.
- [29] Simian Luo, Yiqin Tan, Longbo Huang, Jian Li, and Hang Zhao. Latent consistency models: Synthesizing high-resolution images with few-step inference. *arXiv preprint arXiv:2310.04378*, 2023.

- [30] Simian Luo, Yiqin Tan, Suraj Patil, Daniel Gu, Patrick von Platen, Apolinário Passos, Longbo Huang, Jian Li, and Hang Zhao. Lcm-lora: A universal stable-diffusion acceleration module, 2023.
- [31] Yihong Luo, Siya Qiu, Xingjian Tao, Yujun Cai, and Jing Tang. Energy-calibrated vae with test time free lunch, 2024.
- [32] Chenlin Meng, Yutong He, Yang Song, Jiaming Song, Jiajun Wu, Jun-Yan Zhu, and Stefano Ermon. Sdedit: Guided image synthesis and editing with stochastic differential equations. In *International Conference on Learning Representations*, 2022.
- [33] Chong Mou, Xintao Wang, Liangbin Xie, Jian Zhang, Zhongang Qi, Ying Shan, and Xiaohu Qie. T2i-adapter: Learning adapters to dig out more controllable ability for text-to-image diffusion models. *arXiv preprint arXiv:2302.08453*, 2023.
- [34] Maxime Oquab, Timothée Darcet, Théo Moutakanni, Huy V. Vo, Marc Szafraniec, Vasil Khalidov, Pierre Fernandez, Daniel HAZIZA, Francisco Massa, Alaaeldin El-Nouby, Mido Assran, Nicolas Ballas, Wojciech Galuba, Russell Howes, Po-Yao Huang, Shang-Wen Li, Ishan Misra, Michael Rabbat, Vasu Sharma, Gabriel Synnaeve, Hu Xu, Herve Jegou, Julien Mairal, Patrick Labatut, Armand Joulin, and Piotr Bojanowski. DINOv2: Learning robust visual features without supervision. *Transactions on Machine Learning Research*, 2024.
- [35] Junting Pan, Keqiang Sun, Yuying Ge, Hao Li, Haodong Duan, Xiaoshi Wu, Renrui Zhang, Aojun Zhou, Zipeng Qin, Yi Wang, Jifeng Dai, Yu Qiao, and Hongsheng Li. Journeydb: A benchmark for generative image understanding, 2023.
- [36] William Peebles and Saining Xie. Scalable diffusion models with transformers. *arXiv preprint arXiv:2212.09748*, 2022.
- [37] Dustin Podell, Zion English, Kyle Lacey, Andreas Blattmann, Tim Dockhorn, Jonas Müller, Joe Penna, and Robin Rombach. Sdxl: Improving latent diffusion models for high-resolution image synthesis. *arXiv preprint arXiv:2307.01952*, 2023.
- [38] Alec Radford, Luke Metz, and Soumith Chintala. Unsupervised representation learning with deep convolutional generative adversarial networks. In *ICLR*, 2016.
- [39] Aditya Ramesh, Prafulla Dhariwal, Alex Nichol, Casey Chu, and Mark Chen. Hierarchical text-conditional image generation with clip latents. *arXiv preprint arXiv:2204.06125*, 1(2):3, 2022.
- [40] Robin Rombach, Andreas Blattmann, Dominik Lorenz, Patrick Esser, and Björn Ommer. High-resolution image synthesis with latent diffusion models. In *Proceedings of the IEEE/CVF conference on computer vision and pattern recognition*, pages 10684–10695, 2022.
- [41] Tim Salimans and Jonathan Ho. Progressive distillation for fast sampling of diffusion models. In *International Conference on Learning Representations*, 2022.
- [42] Axel Sauer, Tero Karras, Samuli Laine, Andreas Geiger, and Timo Aila. Stylegan-t: Unlocking the power of gans for fast large-scale text-to-image synthesis. *arXiv preprint arXiv:2301.09515*, 2023.
- [43] Axel Sauer, Tero Karras, Samuli Laine, Andreas Geiger, and Timo Aila. StyleGAN-T: Unlocking the power of GANs for fast large-scale text-to-image synthesis. volume abs/2301.09515, 2023.
- [44] Axel Sauer, Dominik Lorenz, Andreas Blattmann, and Robin Rombach. Adversarial diffusion distillation, 2023.
- [45] Christoph Schuhmann, Romain Beaumont, Richard Vencu, Cade Gordon, Ross Wightman, Mehdi Cherti, Theo Coombes, Aarush Katta, Clayton Mullis, Mitchell Wortsman, et al. Laion-5b: An open large-scale dataset for training next generation image-text models. *Advances in Neural Information Processing Systems*, 35:25278–25294, 2022.

- [46] Jascha Sohl-Dickstein, Eric Weiss, Niru Maheswaranathan, and Surya Ganguli. Deep unsupervised learning using nonequilibrium thermodynamics. In *International conference on machine learning*, pages 2256–2265. PMLR, 2015.
- [47] Jiaming Song, Chenlin Meng, and Stefano Ermon. Denoising diffusion implicit models. *arXiv preprint arXiv:2010.02502*, 2020.
- [48] Yang Song and Prafulla Dhariwal. Improved techniques for training consistency models. In *The Twelfth International Conference on Learning Representations*, 2024.
- [49] Yang Song, Prafulla Dhariwal, Mark Chen, and Ilya Sutskever. Consistency models. 2023.
- [50] Yang Song, Jascha Sohl-Dickstein, Diederik P Kingma, Abhishek Kumar, Stefano Ermon, and Ben Poole. Score-based generative modeling through stochastic differential equations. In *International Conference on Learning Representations*, 2021.
- [51] Patrick von Platen, Suraj Patil, Anton Lozhkov, Pedro Cuenca, Nathan Lambert, Kashif Rasul, Mishig Davaadorj, Dhruv Nair, Sayak Paul, William Berman, Yiyi Xu, Steven Liu, and Thomas Wolf. Diffusers: State-of-the-art diffusion models. <https://github.com/huggingface/diffusers>, 2022.
- [52] Zhengyi Wang, Cheng Lu, Yikai Wang, Fan Bao, Chongxuan Li, Hang Su, and Jun Zhu. Prolicdreamer: High-fidelity and diverse text-to-3d generation with variational score distillation. *arXiv preprint arXiv:2305.16213*, 2023.
- [53] Xiaoshi Wu, Yiming Hao, Keqiang Sun, Yixiong Chen, Feng Zhu, Rui Zhao, and Hongsheng Li. Human preference score v2: A solid benchmark for evaluating human preferences of text-to-image synthesis. *arXiv preprint arXiv:2306.09341*, 2023.
- [54] Zhisheng Xiao, Karsten Kreis, and Arash Vahdat. Tackling the generative learning trilemma with denoising diffusion GANs. In *International Conference on Learning Representations*, 2022.
- [55] Jianwen Xie, Yang Lu, Ruiqi Gao, and Ying Nian Wu. Cooperative learning of energy-based model and latent variable model via mcmc teaching. In *Proceedings of the AAAI Conference on Artificial Intelligence*, volume 32, 2018.
- [56] Jianwen Xie, Zilong Zheng, and Ping Li. Learning energy-based model with variational auto-encoder as amortized sampler. In *Proceedings of the AAAI Conference on Artificial Intelligence*, volume 35, pages 10441–10451, 2021.
- [57] Jianwen Xie, Yaxuan Zhu, Jun Li, and Ping Li. A tale of two flows: Cooperative learning of langevin flow and normalizing flow toward energy-based model. In *International Conference on Learning Representations*, 2022.
- [58] Jiarui Xu, Sifei Liu, Arash Vahdat, Wonmin Byeon, Xiaolong Wang, and Shalini De Mello. Open-Vocabulary Panoptic Segmentation with Text-to-Image Diffusion Models. *arXiv preprint arXiv:2303.04803*, 2023.
- [59] Yanwu Xu, Mingming Gong, Shaoan Xie, Wei Wei, Matthias Grundmann, Tingbo Hou, et al. Semi-implicit denoising diffusion models (siddms). *arXiv preprint arXiv:2306.12511*, 2023.
- [60] Yanwu Xu, Yang Zhao, Zhisheng Xiao, and Tingbo Hou. Ufogen: You forward once large scale text-to-image generation via diffusion gans. *ArXiv*, abs/2311.09257, 2023.
- [61] Zeyue Xue, Guanglu Song, Qiushan Guo, Boxiao Liu, Zhuofan Zong, Yu Liu, and Ping Luo. Raphael: Text-to-image generation via large mixture of diffusion paths. *arXiv preprint arXiv:2305.18295*, 2023.
- [62] Tianwei Yin, Michaël Gharbi, Richard Zhang, Eli Shechtman, Fredo Durand, William T Freeman, and Taesung Park. One-step diffusion with distribution matching distillation. *arXiv preprint arXiv:2311.18828*, 2023.

- [63] Fisher Yu, Ari Seff, Yinda Zhang, Shuran Song, Thomas Funkhouser, and Jianxiong Xiao. Lsun: Construction of a large-scale image dataset using deep learning with humans in the loop. *arXiv preprint arXiv:1506.03365*, 2015.
- [64] Lvmin Zhang, Anyi Rao, and Maneesh Agrawala. Adding conditional control to text-to-image diffusion models. In *Proceedings of the IEEE/CVF International Conference on Computer Vision*, pages 3836–3847, 2023.
- [65] Richard Zhang, Phillip Isola, Alexei A Efros, Eli Shechtman, and Oliver Wang. The unreasonable effectiveness of deep features as a perceptual metric. In *CVPR*, 2018.

Algorithm 1 YOSO training from scratch.

Require: dataset \mathcal{D} , learning rate η , total denoising steps T , total iterations N , distance metric $d(\cdot, \cdot)$, and noise scheduler $\mathcal{Q}(\cdot, \cdot, \cdot)$.

Ensure: optimized models G_θ, D_ϕ .

- 1: Initialize weights $\{\theta, \phi\}$;
 - 2: **for** $i \leftarrow 1$ **to** N **do**
 - 3: Sample noise ϵ from standard normal distribution;
 - 4: Sample data \mathbf{x} from dataset \mathcal{D} ;
 - 5: Sample Timesteps t from 1 to T uniformly.
 - 6: Obtain noisy samples $\mathbf{x}_t = \mathcal{Q}(\mathbf{x}, \epsilon, t)$
 - 7: Obtain less noisy samples $\mathbf{x}_{t-1} = \mathcal{Q}(\mathbf{x}, \epsilon, t-1)$
 - 8: Obtain one-step prediction: $\hat{\mathbf{x}}^t = G_\theta(\mathbf{x}_t, t)$ and $\hat{\mathbf{x}}^{t-1} = G_\theta(\mathbf{x}_{t-1}, t-1)$
 - 9: **# update discriminator**
 - 10: Compute Loss \mathcal{L}_ϕ following Eq. (4).
 - 11: $\phi \leftarrow \phi - \eta \nabla_\phi \mathcal{L}_\phi$;
 - 12: **# update Generator**
 - 13: Compute Loss \mathcal{L}_θ following Eq. (4).
 - 14: $\theta \leftarrow \theta - \eta \nabla_\theta \mathcal{L}_\theta$;
 - 15: **end for**
-

A Broader Impacts

This work presents YOSO, a method that accelerates multi-step large-scale text-to-image diffusion models into a one-step generator. On the positive side, while this is academic research, we believe the proposed YOSO can be widely applied in industry, and its high efficiency can lead to energy savings and environmental benefits. However, when these rapid generation models are manipulated by malicious actors, they can also simplify and accelerate the creation of harmful information. Although our work focuses on scientific research, we will take actions to reduce the harmful information, such as filtering out harmful content in the dataset.

B Limitation

Our model, like most text-to-image diffusion models, may exhibit shortcomings in terms of fairness, as well as in handling specific details and accurately controlling the number of targets. We plan to explore these unresolved issues in the generation field in our future work, in order to enhance the model’s capabilities in text generation, fairness, detail control, and quantitative control.

C Safeguards

The YOSO-SD and YOSO-PixArt- α are trained on the JourneyDB dataset [35], which has undergone rigorous human and machine-based filtering to ensure that there are no harmful or violent images in the dataset. YOSO-LoRA and YOSO-LoRA-V2, on the other hand, were trained using data generated by SDXL-turbo and YOSO-LoRA, respectively. To reduce the risk associated with the models, we utilized the built-in safety checker from diffusers [51] to filter out harmful data.

D Training Algorithm

We present the algorithm for training YOSO from scratch in Algorithm 1.

E Additional Related Work

Text-to-image Diffusion Models. Since Diffusion models have shown a stable training process and are well-suited for scaling up generative models, numerous works have been proposed to extend DMs for text-to-image generation [1, 39, 40, 61]. Latent DMs [37, 40] are widely adopted for high-resolution image and video generation due to their computational efficiency.



(a) w/o quick adaption.

(b) w/ quick adaption.

Figure 7: **One-step** generated images by YOSO-PixArt- α trained with only 5k iterations under different configurations from the same initial noise and prompt.

F The Effect of Quick-Adaption

We present a qualitative comparison between YOSO w/o quick adaption and YOSO w/ quick adaption in Fig. 7. Note that the YOSO and variants here are trained with only 5k iterations. And for YOSO w/ quick adaption, we incorporate the 1k iterations used for quick adaptation into the total 5k training iterations to ensure a fair comparison. As shown in Fig. 7, YOSO w/ quick adaption demonstrates significantly better image quality compared to YOSO w/o quick adaption. The generated images of YOSO w/o quick adaption exhibit over-smoothing and severe artifacts. This indicates that the convergence of direct transition to v-prediction and zero terminal SNR is relatively slower. Additionally, it is worth highlighting that although there are only 5k training iterations, the one-step generation quality of YOSO is already reasonable, which demonstrates the effectiveness and quick convergence of the proposed quick adaption stage and YOSO.

G Experiment Setting Details

G.1 Unconditional Generation Experiments

For the generator, we use the Adam optimizer with $\beta_1 = 0.9$ and $\beta_2 = 0.999$; for the discriminator, we use the Adam optimizer with $\beta_1 = 0.$ and $\beta_2 = 0.999$. We adopt a constant learning rate of $2e-4$ for both the discriminator and the generator. We apply EMA with a coefficient of 0.9999 for the generator. We let the $\lambda_t = \text{SNR}(t)$ and $\lambda_t^{\text{con}} = \frac{1}{\frac{1}{\text{SNR}(t)} - \frac{1}{\text{SNR}(t-1)}}$.

G.2 Text-To-Image Experiments

For the generator, we use the AdamW optimizer with $\beta_1 = 0.9$ and $\beta_2 = 0.999$; for the discriminator, we use the AdamW optimizer with $\beta_1 = 0.$ and $\beta_2 = 0.999$. We adopt a constant learning rate of $2e-5$ for both the discriminator and the generator. We apply gradient norm clipping with a value of 1.0 for the generator only. We use batch size 256. For full fine-tuning, we apply EMA with a coefficient of 0.9999 for the generator. For LoRA fine-tuning, we apply EMA with a coefficient of 0.999 for the generator. Generally, the training is done within 30k iterations for full fine-tuning, while within 5k iterations for LoRA fine-tuning. We let the $\lambda_t = \text{SNR}(t)$ and $\lambda_t^{\text{con}} = \frac{1}{\frac{1}{\text{SNR}(t)} - \frac{1}{\text{SNR}(t-m)}}$.

For full fine-tuning, we train YOSO on the JourneyDB dataset [35], by resizing to 512 resolution. And we only use the square image. For LoRA fine-tuning, we use the caption of the JourneyDB dataset [35] to generate data for training, we only generate one image for one caption.